Dynamic and Static Characterization of Recent Crack Arrest Tests of Navy and Nuclear Steels

James A. Joyce[1, a], R.E. Link[1,b], C. Roe[2,c] and J.C. Sobotka[3,d]

[1]US Naval Academy, Annapolis MD USA

[2]Naval Surface Warfare Center, Carderock Division, Bethesda MD USA

[3]Civil Engineering Department, University of Illinois, Urbana IL USA

[a]jaj@usna.edu, [b]link@usna.edu, [c]charles.roe@navy.mil, [d]sobotkajc@gmail.com

Keywords: Crack arrest, fracture toughness, dynamic crack arrest, stress intensity factor, J-integral, crack arrestor strakes, ductile-to-brittle transition, initiation toughness, HSLA100, HY100, European round robin, dynamic computational analysis, ASTM E1221, ASTM E1921.

Abstract. Crack arrestor strakes are used in U.S. Navy warships and have eliminated large scale cracking that might result in catastrophic failure of the ship hull and structure. Present U.S. Navy vessels utilize HY80 or HY100 steels for the crack arrestor strake materials and fabricating hull structures with a combination of the HY steels and more common marine structural steels is very expensive and time consuming. Determining the exact toughness required to arrest a running crack in a navy vessel is beyond present fracture mechanics capabilities, but a comparison of the crack arrest toughness of the existing HY steels and candidate replacement steels like the newer HSLA 100 steel now is possible. It is very difficult to do laboratory crack arrest tests on these high toughness steels because the crack initiation toughness is so high that it is difficult to initiate a running crack in a laboratory specimen and even more difficult to obtain a crack arrest under conditions where the experimental results can be characterized by present fracture mechanics analysis techniques. Specifically, if the existing ASTM E1221 standard is used for these materials, one is required to use large specimens, on the order of 0.5 to 1 m or larger in scale, to test far below the normal ship operating temperatures, and the results are likely still to be invalid because of crack branching, excessive crack growth, insufficient crack growth or alternately no initiation. Similar difficulties are encountered in crack arrest testing of nuclear pressure vessel steels. While test temperature can be higher, they are still far below the temperatures expected for the nuclear pressure vessel applications. The ASTM E1221 type test is not applicable to these materials at temperatures of interest in the mid to upper transition. The U.S. Nuclear Regulatory tests conducted by Oak Ridge National Laboratory in 1985 utilized large single edge notched tension specimens to obtain crack arrest data high in the ductile-to-brittle transition, but because of the high initiation toughness and the rising K-field present in this geometry, a thermal gradient across the specimen was required to arrest the crack in the 1 meter wide specimen. The very large size of the specimens caused high costs which allowed only a small number of tests to be run, resulting in a large uncertainty in the results due to the inherent variability of crack arrest toughness. The objective here is to utilize recent developments in fracture mechanics and in computational tools to improve test procedures so that crack arrest information can be obtained more readily for both navy and nuclear steels. Smaller specimens are utilized to reduce costs and to allow more specimens to be tested, precracked specimens are utilized allowing the cleavage initiation to be predicted using newly developed Master Curve techniques so that both crack initiation and crack arrest data can be obtained from each test sample, and dynamic computational analysis is used to assure the accuracy of the test result as well as to compare with the E1221 style static analysis. Tests are also presented on two specimen geometries to obtain at least a first assurance that the results are comparable across test geometries and might then also be applicable in the structural application of interest.

Background

Crack arrest testing was reinitiated to attempt to determine if a newly available HSLA100 steel could be substituted for the HY100 presently utilized in U.S. Navy surface warships as crack arrester strakes. The change was desired to reduce the cost of welding the crack arrestor strakes into the ship structure which requires a complex procedure of preheating and post heating for the HY100 steel but a much less complex procedure for the HSLA100 steel. Successful crack arrest tests have never been conducted on the HY100 steel. Exactly how much crack arrest toughness is required to stop a crack in a U.S. Navy structure has never been determined quantitatively. The crack arrest tests conducted in this study were done to compare the crack arrest capacity of samples of the two candidate materials.

The reasons to reinitiate crack arrest tests on nuclear pressure vessel materials are somewhat different than those of interest to the U.S. Navy. The materials utilized in commercial nuclear power plants have high resistance to cleavage crack initiation and cannot be tested using the procedures in ASTM E1221 accept at test temperatures far below those of the typical application. Large scale crack arrest tests were conducted by the U.S. Nuclear Regulatory Commission (USNRC) during the 1980s. The tests involved initiating cleavage cracks in large single edge notched tension panels and arresting the cracks by providing a thermal gradient. These tests are described in references [1] and [2]. Recently the USNRC has moved to probabilistic fracture mechanics and this has meant that there is a finite probability that cleavage cracks can initiate in nuclear pressure vessels and it is necessary to estimate the probability of crack arrest under typical operating conditions. This has caused a renewed interest in crack arrest tests and crack arrest test conditions in the USNRC research program.

In this study the two Navy materials are thus compared against each other directly to demonstrate that the switch to the newer HSLA material is strongly supported by the crack arrest results. Since these results were also carried out in both CCA (compact crack arrest) and SE(T) (single edge notched tension) geometries they also provide evidence that the test results are at least somewhat independent of the specimen geometry being utilized. The nuclear steel results demonstrate the applicability of the techniques developed here to the crack arrest testing of such steels. In both cases, the availability of both dynamic and static crack arrest stress intensity factor results allows an estimation of the magnitude of error involved in using the static analysis as in ASTM E1221 test procedure

Analysis

The ASTM E1221 Method. The ASTM E1221 standard utilizes a static analysis of the compact crack arrest specimen to obtain an estimate of the crack arrest fracture toughness, K_{Ia}, a short time after crack arrest (about 1 ms). K_{Ia} is inferred from the crack mouth opening displacement measured at crack arrest using the relationship:

$$K_{Ia} = E\, d_a\, f(x) \frac{\sqrt{B/B_N}}{\sqrt{W}} \tag{1}$$

where: $f(x) = (1-a/W)^{0.5}\left[(0.748 - 2.176(a/W) + 3.56(a/W)^2 - 2.55(a/W)^3 + 0.62(a/W)^4\right]$

with: a = crack length at crack arrest,
W = specimen width,
B = specimen thickness,
B_N = specimen thickness at the crack plane,

E = material elastic modulus,
d_a = crack mouth opening displacement at crack arrest.

To account for plastic crack opening displacement (CMOD) included in this measurement a cyclic loading process is used and the crack mouth opening displacement used in Eq. 1 is obtained from:

$$d_a = 0.5\left[\delta_o + \delta_a - (\delta_p)_1 - (\delta_p)_{n-1}\right] \quad (2)$$

where: δ_o = CMOD at the onset of unstable crack growth,
δ_a = CMOD approximately 0.1 s after crack arrest,
$(\delta_p)_1$ = CMOD offset at the end of the first cycle,
$(\delta_p)_{n-1}$ = total CMOD offset at the start of the last cycle.

Based on work by Kalthoff and others [3][4] it is assumed that the resulting crack arrest toughness is a conservative estimate of the true dynamic crack arrest toughness, but the degree of conservatism is not known.

The relatively small specimen size and the constant temperature regime used in the E1221 method restricts the application of the method to materials which have a modest initiation toughness and a small drop between initiation toughness and crack arrest toughness. Brittle weld beads have been used successfully in some cases to initiate a growing crack which propagates into the test material and arrests. Prior work on HY and HSLA steels had shown that this technique was not likely to be successful with the crack instead turning at the weld interface and failing to propagate into the specimen ligament.

These materials and many other steels are not amenable to crack arrest testing using E1221 because they have a relatively high resistance to cleavage fracture initiation and a much lower crack arrest toughness. A schematic comparison of fracture initiation and arrest behaviors that allow crack arrest - Material A, or disallow crack arrest - Material B, tested using the E1221 method is shown schematically in Figure 1. For Material A, a typical cleavage crack initiation K_{Ji} value results in a crack arrest (K_a) value that is above the material lower shelf and corresponds to a change in stress intensity corresponding to a modest crack jump in the compact crack arrest specimen. For a material like Material B, low K_{Ji} values result in cracks that do not arrest until a/W > 0.8 while higher K_{Ji} values do not initiate cleavage cracks, so in either case, no crack arrest toughness can be measured. Additional difficulties that plague E1221 type crack arrest tests are the tendency of the growing crack to turn out of the specimen centerplane, a problem that seems to be most severe in the compact, wedge loaded specimen configuration used in the E1221 procedure.

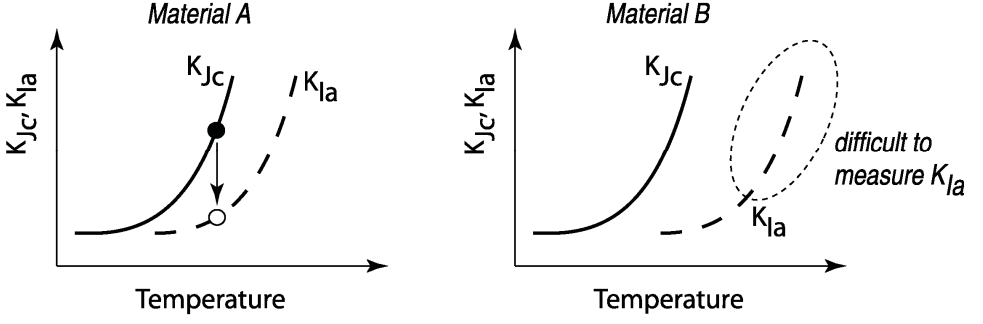

Figure 1 Schematic comparison of fracture toughness transition curves for two hypothetical materials with different shifts between the crack initiation and arrest fracture toughness

Crack Arrest Master Curve. Laboratory crack arrest tests can only be conducted over a narrow temperature range which is near the mid transition for the ferritic steel's ductile-to-brittle transition for cleavage initiation and then hopefully only slightly above the lower shelf for the steel's crack arrest toughness transition. This case was presented schematically in Fig. 1a, above. Transferring test results obtained over this range of temperatures to the application requires a curve fitting and extrapolation procedure of some type. A recent proposal of Wallin and Rintamaa [5], based on the cleavage initiation Master Curve, involves fitting the experimentally measured K_{Ia} data with an equation of the form:

$$K_{Ia(med)} = 30 + 70\exp\left[0.019(T - T_{KIa})\right] \tag{3}$$

where T_{KIa} is the temperature where the median K_{Ia} = 100 MPa√m. The crack arrest reference temperature can be calculated using a maximum likelihood approach from [6]. This fitting procedure is different from that specified in ASTM E1921 because the data are assumed to follow a log-normal distribution rather than a Weibull distribution.

Alternative Crack Arrest Tests. Alternative crack arrest tests have been developed to obtain crack arrest toughness for these high initiation toughness materials. The large scale tests on a nuclear pressure vessel steel conducted by the U.S. Nuclear Regulatory Commission (USNRC) during the 1980s used a temperature gradient to arrest the crack and utilized single edge notched tensile specimens which exhibit a rising K-field with crack extension[1][2]. A thermal gradient was used to establish a toughness gradient such that the material toughness increased with crack length. The brittle crack was initiated in the low temperature/low toughness region and propagated into increasing warmer (tougher) material until it arrested. Tests were conducted on an HY80 steel by Gudas [7] using a large planar size compact crack arrest geometry which also included a thermal gradient to arrest the crack. The USNRC tests were generally more successful since the crack stayed in the original notch plane in most cases.

Experiments

Materials Description. The materials used in this investigation were a 19 mm thick, HSLA-100, Composition 3, steel plate, a 25.4 mm thick HY-100 steel plate and a DIN 22NiMoCr37 pressure vessel steel forging (the Euro forging), which is similar to an A508 Class 3 pressure vessel steel, approximately 240 mm thick. The chemical composition of these three steels and the room temperature tensile mechanical properties are listed in Table 1 and Table 2. Fracture toughness tests of each plate were conducted to determine the reference temperature, T_o, in accordance with ASTM E1921. For the HSLA-100 plate, seven 3/4T, C(T) specimens (W=38mm, B=18mm) were tested at a temperature of -160°C. Eight 1T, C(T) specimens of the HY-100 steel plate were tested at -96°C. The reference temperature, T_o was determined to be -166°C for the HSLA-100 plate and -124°C for the HY-100 plate. For the Euro forging material the reference temperature was taken from Wallin [8] with a conscious eye toward the extensive inhomogeneity study done on this material by Joyce [9]. For this material, an average T_o from the extensive European round robin was shown to be -94°C, but the variation resulting from the large section size of this forging gives a range of reference temperatures from -72°C to -125°C.

Table 1 Chemical composition of the HSLA-100, HY-100, and Euro forging steels.

Element	HSLA-100, Comp. 3	HY-100	Euro Forging
C	0.05	0.15	0.21
Mn	0.82	0.26	0.82
P	0.010	0.008	0.003
S	0.003	0.003	0.004
Si	0.35	0.27	0.24
Cu	1.61	0.12	0.049
Ni	3.41	2.62	0.79
Cr	0.55	1.53	0.003
Mo	0.60	0.37	0.56
N	0.008	0.015	--
Cb	0.03	<0.002	--

Table 2 Room temperature tensile mechanical properties for the HSLA-100, HY-100, and Euro forging steels .

	HSLA-100, Comp. 3, Plate GQN	HY-100, Plate	Euro Forging
Ultimate Tensile Strength, MPa	827	896	612
Yield Strength, MPa	765	731	470
Elongation in 51 mm, %	37	23	--
Reduction in area, %	60	74	70

Specimen Details

SE(T) Specimens. Single edge cracked tension specimens (SE(T)) as shown in Figure 2 were used for tests on the HSLA-100 and HY-100 steels. The SE(T) were pin-loaded specimens with a width, W = 152 mm and an initial crack length, a_0 = 38 mm, with a_0/W = 0.25. The specimen length between the pinholes was 720 mm and the reduced section in the center of the specimen was 300 mm long. The specimens were 19 mm thick for the HSLA-100 plate and 25 mm thick for the HY-100 plate. A fatigue precrack was extended from the machined notch to the desired initial crack length of 38 mm. Precracking was conducted by loading the specimen in three-point bending and K_{max} was less than 20 MPa-$m^{1/2}$. All specimens were side-grooved 10% of the specimen thickness on each face after precracking.

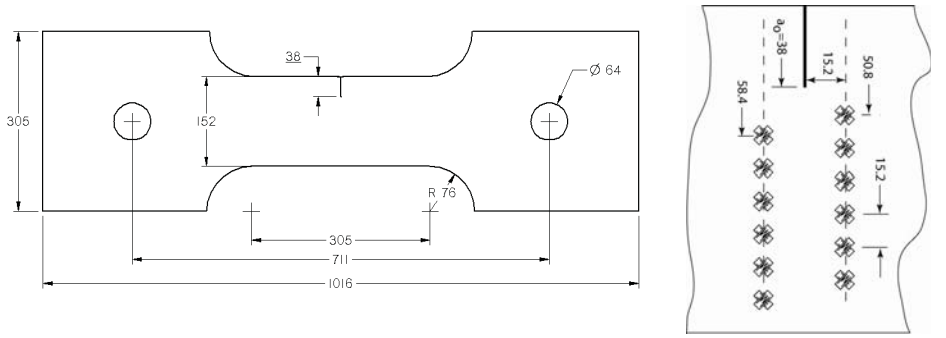

Figure 2 SE(T) specimen drawing of showing the pattern of rosette gages used to measure the crack velocity.

CCA Specimens. Compact crack arrest specimens were used in this study for the HSLA-100 steel and for the Euro forging. The large difference between T_o and T_{Kla} for the HY-100 steel made this specimen unsuitable for this material. Two sizes of this specimen were utilized, the W = 120 mm size described above and a smaller W = 50 mm size. These specimens were tested isothermally, enclosed in a test chamber, and wedge loaded as is typical of ASTM E1221 tests, see Figure 3. Tests were conducted on these specimens according to E1221 using pre-cracks introduced in the specimens according to the specifications of E1921. Strain gage rosettes were applied to both surfaces of some of the W=120 mm specimens, offset above and below the crack plane, to obtain crack velocity data for use in the dynamic FEA analysis of these specimens.

Figure 3 Test apparatus for an isothermal, wedge loaded, CCA specimen, W=50mm (shown without the specimen hold-down and chamber cover).

Description of the Test Procedure. In the work conducted as part of this study the SE(T) geometry was chosen so that rapidly extending crack would be more likely to stay in the desired crack plane. Since the stress intensity factor increases with crack extension in this geometry, as

shown in Figure 4, it was clear that a steep temperature gradient would then be required to arrest the crack after limited crack growth. Smaller specimen sizes were required to keep the budget reasonable. Advances in computational capabilities, however, did promise to allow a full 3D

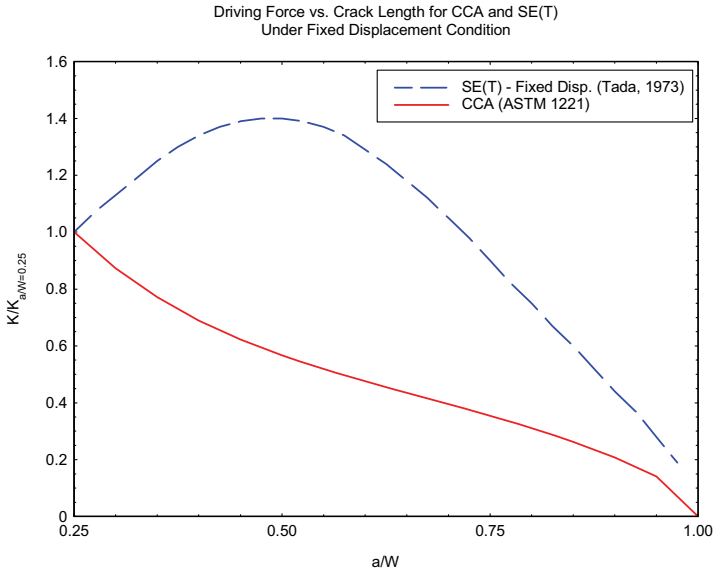

Figure 4 Stress intensity factor versus crack length for CCA and SE(T) crack arrest specimen geometries.

dynamic analysis of the growing crack which had not been practical for previous crack arrest analyses.

The dynamic finite element analysis of the SE(T) specimen required specification of the crack tip position as a function of time so it was necessary to measure the crack tip location history during the brittle fracture event. The specimens were instrumented with 12 strain gage rosettes placed along lines parallel to the crack plane a distance of 15 mm above and below the crack plane. This offset distance was necessary to keep the gages away from the influence of three-dimensional effects due to the side grooves and to remain outside of the crack tip plastic zone. The strain gages were positioned as shown in Figure 2 with the gages above the crack plane offset by 0.05W from those below the crack plane to give an effective spacing of 0.05W along the crack path. The gages were two-element stacked rosettes with the active grids oriented at 90° to each other. The rosettes were oriented with their active grids at ±45° to the crack path and each rosette was wired into adjacent arms of a Wheatstone bridge to record the difference between the individual strain signals, $\varepsilon_{y'y'} - \varepsilon_{x'x'}$. This configuration provides cancellation of thermally-induced strains and the characteristic response of the rosette to the passing crack tip exhibits several features which permit determination of the crack tip position as a function of time [10].

The strain gages were connected to high frequency bridge amplifiers for signal conditioning and the amplifiers were connected to digital storage oscilloscopes. The transient strain data was captured at 1μs intervals during the run-arrest event.

A thermal gradient was established by a combination of heating and cooling opposite edges of the specimen. A stainless steel chamber was fabricated from thin sheet to hold liquid nitrogen for

cooling the notched edge of the specimen and was secured to the specimen using mechanical fasteners and cryogenic adhesive. An aluminum block with four electrical resistance heaters was attached to the back face of the specimen and a variable transformer was used to control the power supplied to the heaters. A series of 10 thermocouples were uniformly spaced along the specimen width just above the side groove. The thermocouples were peened into small holes drilled into the surface of the specimen and were used to monitor the temperature gradient and determine when an equilibrium linear gradient was achieved.

A typical temperature gradient across the test section of a specimen at the commencement of testing was approximately 1°C/mm with a maximum deviation 7°C from a linear fit. Once a linear gradient was established, the absolute temperature level could be adjusted by varying the power to the electrical heaters but it was not possible to independently control the slope of the temperature distribution. In addition to the transient strain signals, the applied force and crack mouth opening displacement were recorded. A photograph of fully instrumented specimen is shown in Figure 5.

Dynamic SE(T) Computational Model

Finite element analysis was used to model the crack arrest tests and to determine the dynamic crack arrest fracture toughness. The finite element code, WARP3D, was used to perform the analyses[11]. Plane strain and 3-D models of the specimen were used in this investigation. A detailed description of the development and validation of the models used is available in previous publications [12][13]. The material constitutive behavior employed a von Mises yield criterion with isotropic hardening. A power-law, visco-plastic material model available in the WAPR3D code was used to characterize the strain-rate sensitivity of the steel. An isothermal, visco-plastic stress-strain curve, corresponding to the specimen temperature at the point of crack arrest was used. Crack growth was modeled by using a prescribed node-release technique wherein an equivalent reaction force replaced the displacement constraint at the crack tip and the reaction force was linearly relaxed to zero over a fixed number of time steps. This is a generation-mode analysis where the crack length vs. time history is explicitly enforced as a known boundary condition.

The domain integral technique was used to calculate the dynamic J-integral averaged over the crack front. Computed J values were domain independent for analyses incorporating linear-elastic material models. This was not true for elastic-plastic analyses. Domains that pass thru the plastic wake exhibit path dependence due to the non-proportional unloading in the plastic wake. Consequently, domains were specified to be remote from the crack tip so that they completely enclosed the plastic wake behind the advancing crack. J values calculated using remote domains were path independent for the linear and elastic-plastic analyses. A through- thickness average value of J was used in all of the 3D results reported herein.

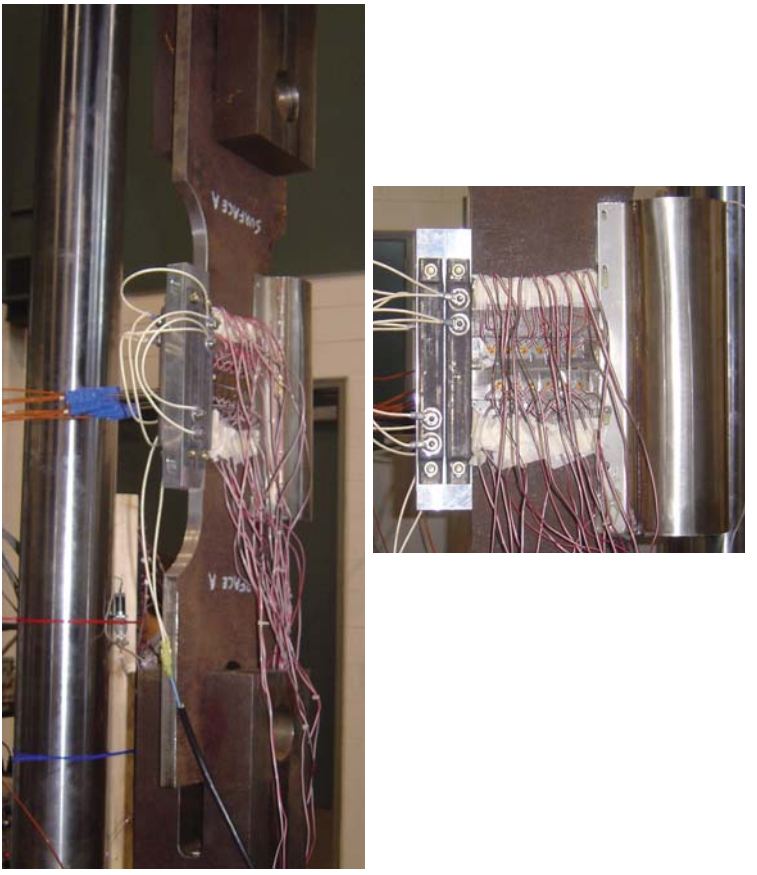

Figure 5 An instrumented SE(T) crack arrest specimen mounted in the test machine. A heater is mounted on the near edge and the liquid nitrogen container is along the far edge of the specimen.

The J-integral was converted to an equivalent stress intensity using the relationship:

$$J = \mathcal{G} = \frac{K^2\left(1-\upsilon^2\right)}{E} A(\mathrm{v}) \tag{4}$$

where E is the elastic modulus, ν is Poisson's ratio and A(v) is a universal function of the crack velocity, v, given in [14] as:

$$\mathrm{A(v)} = \frac{\mathrm{v}^2 \alpha_d}{(1-\nu)c_s^2 D} \tag{5}$$

where $D=4\alpha_d\alpha_s - (1+\alpha_s^2)^2$ and $\alpha_d = \sqrt{1-\mathrm{v}^2/c_d^2}$, $\alpha_s = \sqrt{1-\mathrm{v}^2/c_s^2}$ and c_d and c_s are the elastic dilatational and shear wave speeds, respectively. A(v) goes to 1 as the crack velocity goes to zero and increases monotonically with crack speed. For the range crack velocities observed in these

tests, the A(v) term is approximately 1.01, providing a negligible effect on the conversion between J and K and was not included in the calculations of the dynamic stress intensity factor for this study.

In all of the results presented in this paper, the dynamic stress intensity factor is only computed at time steps corresponding to a complete increment of crack extension - that is, when restraint forces at the crack tip node have been completely relaxed to zero.

Some general observations can be made about the dynamic response of the SE(T) specimen based on the previous publications. Immediately upon initiation, the stress intensity factor drops on the order of 10-45%, the exact amount of reduction depends upon the crack speed. The reduction in the stress intensity is a result of stored elastic energy being converted into kinetic energy. Higher crack velocities lead to lower values for the crack driving force during dynamic crack propagation. As the crack propagates at the prescribed velocity, the driving force increases gradually but is well below the quasi-static, fixed grip solution. It is clear that a static analysis is of little use for predicting the dynamic response of the SE(T) specimen. Immediately after the last increment of crack growth corresponding to arrest, the stress intensity exhibits a step-like, rapid increase with some oscillation and then continues to rise more gradually as the specimen begins to ring. The stress intensity at crack arrest is slightly influenced by the assumed crack velocity.

Preliminary analyses were performed using both plane strain and 3-D meshes to quantify the effects of element size along the crack plane, the number of unload steps per increment of crack growth, the modeling of the pin-loading, crack velocity and material constitutive models on the specimen response and the results of these analyses are reported by Link[12]. The model used here was chosen to minimize the effects of these on the results of the analyses.

The initial load was applied to the FE model by specifying a fixed displacement of the rigid loading pin that produced the initiation force measured in the experiment. The pin displacement was held constant during the simulation and the contact condition at the pin was included in the analysis. Dynamic crack growth was modeled by prescribed release of the crack tip nodal reaction forces over a series of ten time steps per element of crack advance. In these analyses, the crack propagated at an assumed constant velocity controlled by the time step from initiation to the second to last increment of crack growth. The crack velocity decreased by a factor of two at the start and midpoint of the final increment of crack growth.

Dynamic strain data throughout the run-arrest event was recorded for each test and used to estimate the crack speed for input into the finite element analysis of each individual test. The strain signals recorded for an HSLA-100 specimen GQN-TL5, shown in Figure 6 show the typical response of the rosettes to the rapidly propagating crack. The strain signals peak as the crack approaches the gage position, and then go from positive to negative as the crack passes below the gage and produce a negative peak before gradually increasing their output. Both the time of the zero crossing of the strain signal and the negative peak are features which can be used to locate the crack tip position [10].

The location of the crack tip relative to the zero crossing and the negative peak in the strain response were determined from three-dimensional, dynamic finite element analyses of the SE(T) specimen with the crack propagating at a constant velocity. While the magnitude of both the positive and negative peak are influenced by the crack speed and the value of the dynamic stress intensity, K_{ID}, the location of the zero crossing is only slightly affected and the negative peak location is relatively insensitive to the crack speed for the range of crack speeds observed in these tests.

The time of the zero crossing and the negative peak from each rosette were used to estimate the crack tip position as a function of time during each test and to compute the velocity as shown in Figure 7. The data was well represented with a linear fit which implies a constant crack speed of 353 m/s for this specimen. The crack tip position vs. time results for all of the HSLA-100 specimens showed similar linear trends with crack speeds in the range of 216-400 m/s for the

HSLA-100 specimens. The HY-100 specimens had higher crack speeds, in the range of 480-685 m/s at initiation and several appeared to propagate at lower velocity as the crack advanced. In cases where the crack speed appeared to slow with crack extension, two or three stages of constant velocity crack growth were assumed in the FE models.

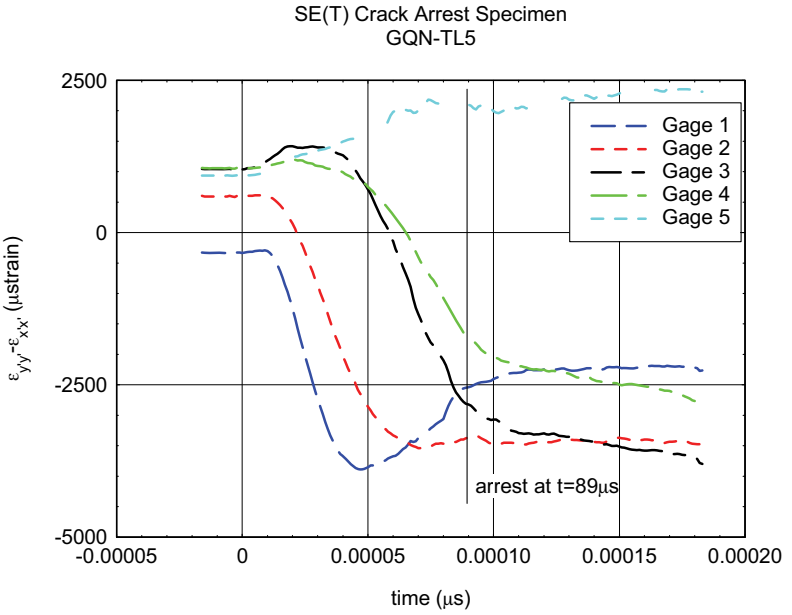

Figure 6 Dynamic strain data throughout the run-arrest event as recorded for an HSLA-100 specimen,GQN-TL5.

The crack speed and initiation load together with the initial and arrested crack lengths were used as boundary conditions for the generation-mode analysis of the dynamic crack propagation and arrest event. The predicted dynamic crack driving force history for specimen GQN-TL5 is plotted in Figure 8. The specimen response shows the driving force dropping immediately after initiation and then gradually increasing as the crack advanced until crack arrest occurred with the driving force making a rapid increase at the moment of arrest. After the crack arrests, the driving force continues to increase and oscillate as the remaining energy in the specimen oscillates between strain energy and kinetic energy. As observed on the fracture surfaces, the driving force was often sufficient to initiate ductile tearing after the cleavage crack arrested but this was not modeled in the finite element simulations.

The finite element analyses were validated by comparing the predicted strain response with the experimentally measured strain signals. In some cases there was excellent agreement as shown in Figure 9 for specimen GQN-TL8 while in other cases the agreement was only satisfactory as shown in Figure 10 for specimen GQN-TL5. Some possible reasons for the difference between the predicted and measured strains may be a result of the crack tunneling and non-planar crack growth that was observed on the fracture surfaces. The finite element analyses assumed uniform, straight crack fronts and planar crack growth. The crack tip propagated at a constant velocity in the finite element analysis, which may be a simplification of the physical behavior.

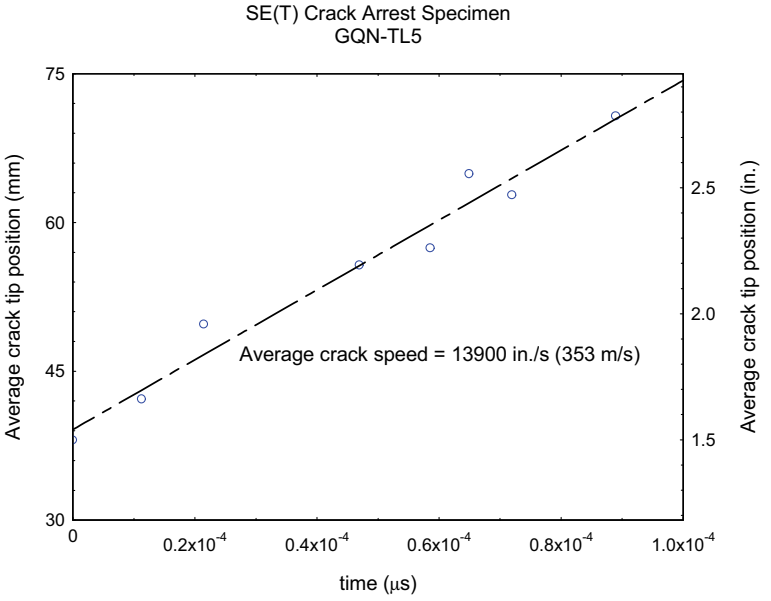

Figure 7 The crack tip position as a function of time for HSLA-100 specimen GQN-TL5.

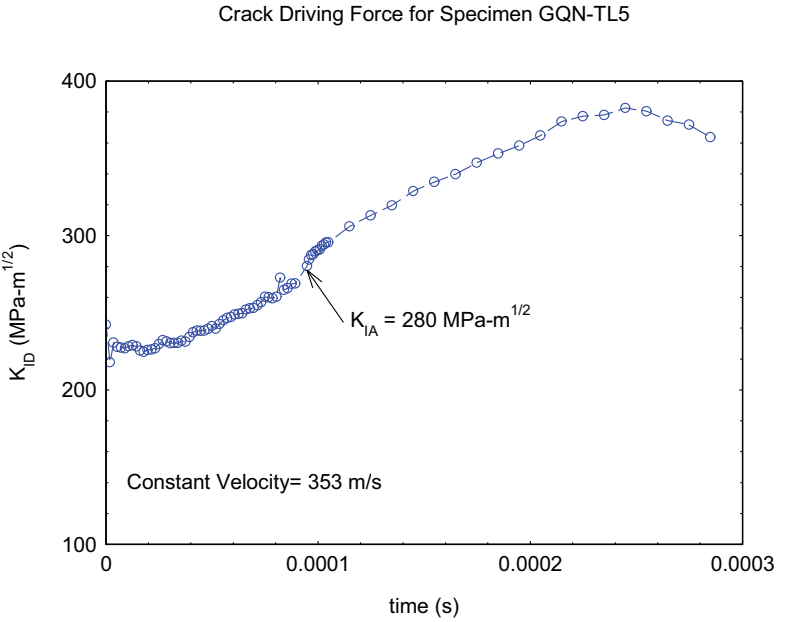

Figure 8 Predicted dynamic crack driving force as a function of time for HSLA-100 specimen GQN-TL5.

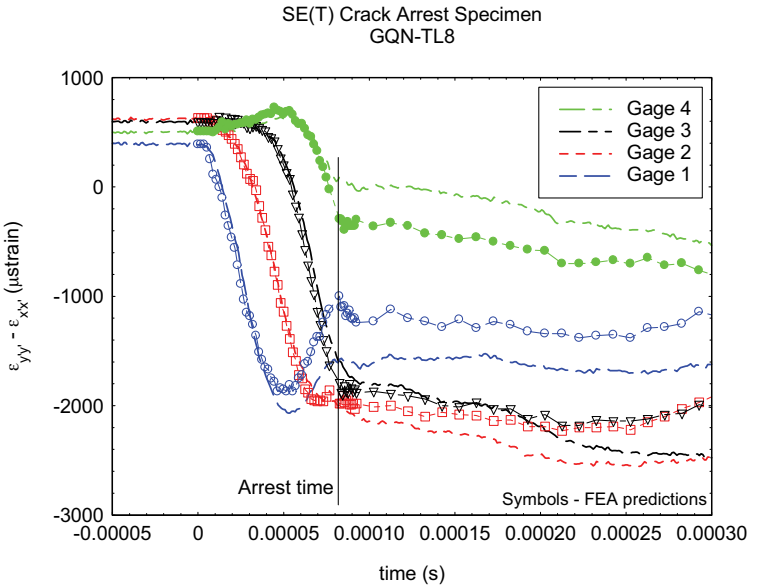

Figure 9 Comparison of the measured and predicted (symbols) transient strain gage rosette response for HSLA-100 specimen GQN-TL8 showing excellent agreement.

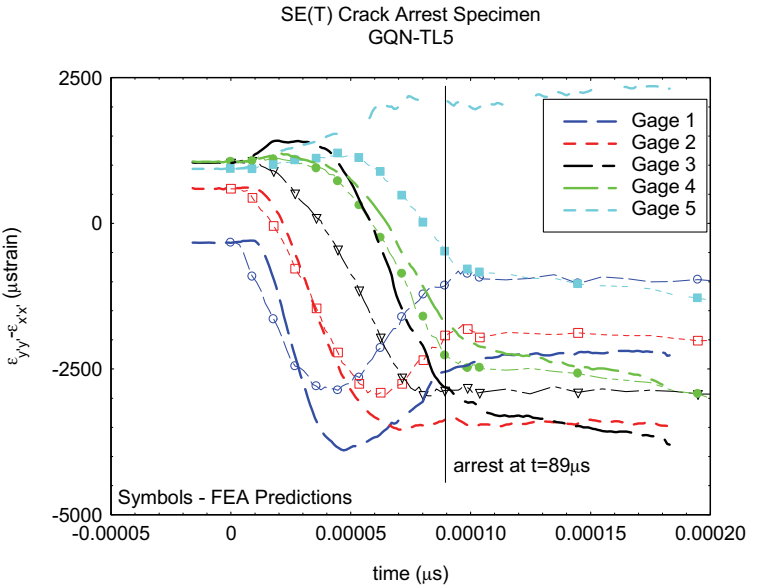

Figure 10 Comparison of the measured and predicted (symbols) transient strain gage rosette response for HSLA-100 specimen GQN-TL5 showing good agreement for some gages and only moderate similarity for others.

Dynamic Analysis of the CCA Specimen Geometry

Compact crack arrest specimens were tested in order to investigate the effect of specimen geometry (SE(T) vs. CCA) on the crack arrest toughness and to further investigate any differences between the static analysis used in E1221 and the dynamic finite element analysis procedure used in the SE(T) specimens. In order to compare the dynamic analysis of the SE(T) specimens to the static analysis of E1221, CCA specimens typical of E1221 were strain gaged and tested using the methodology of E1221. The results were analyzed in accordance with the static analysis described in E1221 as well as a full 3-D dynamic analysis using finite elements. The CCA specimens were wedge loaded and conducted without a thermal gradient but strain gages were used to measure the crack speed and position during the run arrest event. The HSLA-100 material was chosen initially for these tests because of the small difference measured between T_o and T_{KIa}, which appeared to allow the use of W = 120 mm CCA specimens for E1221 type tests. These results will be discussed in more detail below.

The finite element grid used to analyze the CCA specimen geometry is shown in Figure 11 and contained approximately 22000 nodes, 17500 elements. It had 5 layers of elements through the half-thickness and the elements along the crack plane were 0.5 mm long. The analysis was run in a manner largely consistent with what had been done previously for the SE(T) specimens. Computational studies examined the effect of the acceleration profile over the final crack growth increment. These studies determined that the dynamic value of the crack arrest toughness was less sensitive to the shape of the acceleration profile 0.5 μs after the release of all reactions forces along the crack plane. Consequently, all computational analyses of the CCA specimens defined the value of K_{IA} in this manner.

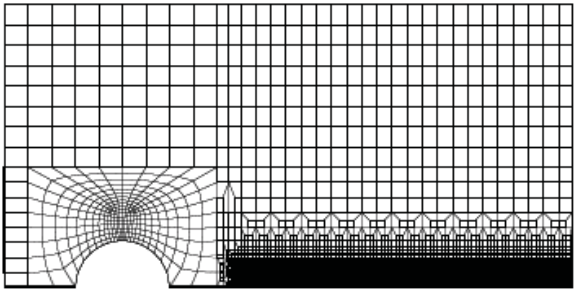

Figure 11 Finite element mesh used for CCA specimen.

Discussion of the Results

Navy Structural Steels The results of the HSLA100 and HY100 SE(T) specimens are presented in Table 3 and Table 4 and in Figure 12 and Figure 13. A first observation is that for the HSLA and HY100 tests, dynamic strain data was successfully captured in 15 of the 16 tests. For the HSLA100 steel, a rather small shift, 31°C, was observed between the reference temperatures for crack initiation and crack arrest with T_o = -166°C and T_{KIa} = -135°C. The HY100 steel exhibited a much greater shift in the reference temperatures with T_o = -124°C and T_{KIa} = -64°C for a shift of 60° C. Figure 14 shows a direct comparison of the initiation and arrest master curves for these two candidate crack arrestor strake materials showing the HSLA material to be much superior since its arrest master curve is elevated, not just with respect to the HY100 crack arrest master curve but also lying above the HY100 cleavage initiation master curve.

Significant cleavage crack propagation occurred in all tests with no evidence of crack branching. Crack propagation ranged from 11 to 36 mm in the HSLA-100 steel specimens and 38 to 80 mm in the HY-100 steel specimens. More significant crack tunneling was present in the tougher HSLA100 material than was observed in the HY100 steel. Abrupt arrest was observed in all cases. For the HY100 steel the initial crack arrest was followed in most instances by re-initiation and arrest and often included at least one segment of ductile tearing. The lower fracture toughness demonstrated by the HY100 steel was readily apparent by observations of the longer crack jumps, more limited crack tunneling and improved in-plane behavior of cleavage crack in comparison with that of the typical HSLA100 specimen.

Table 3 Summary of crack arrest results for HSLA-100 SE(T) specimens in this investigation.

Specimen	Initial crack size, a_0, mm.	Arrested crack size, a_0, mm.	Initiation toughness, K_{init}, MPa-$m^{½}$	Avg. crack speed, m/s	Arrest Temp., T_{arrest}, °C	Arrest toughness, K_{IA}, MPa-$m^{1/2}$
GQN-TL1	38.2	66.5	215	406	-73	274
GQN-TL2	39.0	66.9	132	394	-93	158
GQN-TL3	41.3	52.9	151	216	-92	155
GQN-TL4	38.0	74.9	192	406	-89	236
GQN-TL5	38.0	70.7	242	356	-72	280
GQN-TL6	38.5	69.3	308	381	-60	318
GQN-TL7	37.8	73.8	359	406	-63	378
GQN-TL8	37.9	66.2	127	356	-93	154

Table 4 Summary of crack arrest results for HY-100 SE(T) specimens in this investigation.

Specimen	Initial crack size, a_0, mm	Arrested crack size, a_0, mm.	Initiation toughness, K_{init}, MPa-$m^{1/2}$	Avg. crack speed, m/s	Arrest Temp., T_{arrest}, °C	Arrest toughness, K_{IA}, MPa-$m^{1/2}$
HY100-404	36.8	103.0	109	596	-27	148
HY100-405	38.7	118.7	86	635*	-27	115
HY100-406	38.9	88.3	108	701	-36	137
HY100-408	38.9	101.1	118	749	-29	145
HY100-409	40.3	114.5	152	635	-27	206
HY100-410	38.9	86.8	120	483	-42	154
HY100-411	39.5	96.9	181	541	-27	236

* Assumed average crack speed. No strain data for this test.

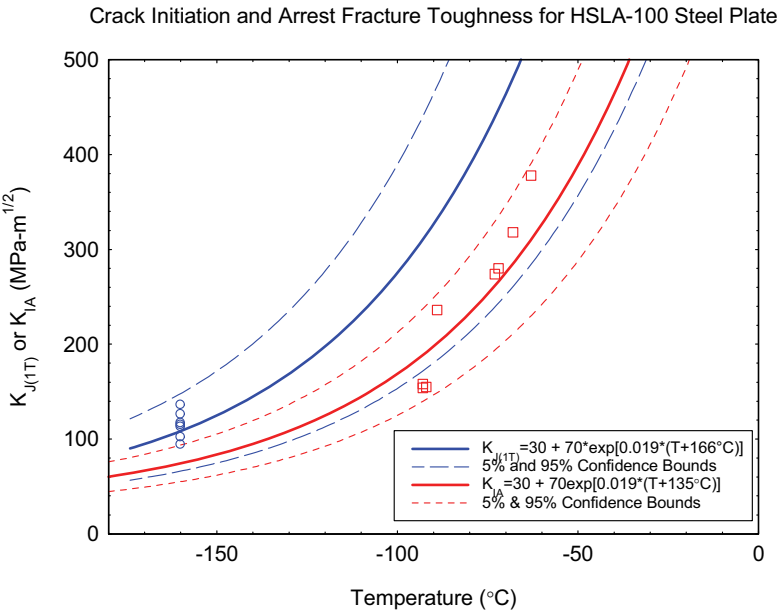

Figure 12 Crack initiation and crack arrest master curves for the HSLA-100 steel plate.

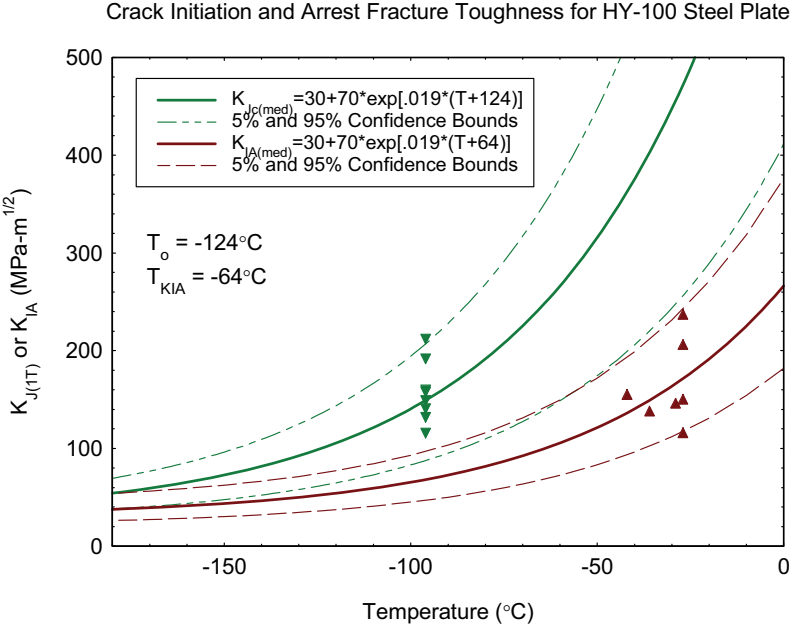

Figure 13 Crack initiation and crack arrest master curves for the HY-100 steel plate.

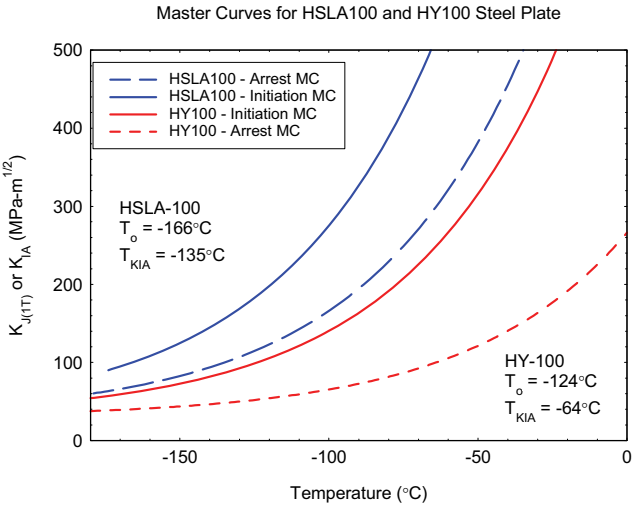

Figure 14 Comparison of initiation and arrest master curves for the two Navy crack arrest materials.

CCA Test Results. The observation from the SE(T) specimen tests that for the HSLA100 steel a shift of only 31°C (T_o = -166°C and T_{KIa} = -135°C) was present between the cleavage initiation master curve and the crack arrest master curve suggested that crack arrest tests using ASTM E1221 might be successful for this steel. Furthermore, this afforded an opportunity to validate the static analysis methodology of E1221 by performing a dynamic analysis of the CCA specimen geometry. This would provide a direct comparison of crack arrest properties between the SE(T) and CCA geometries and would also allow an estimate of the degree of conservatism present in using the static K analysis as is done in the E1221 standard, i.e. the use of Eq. 1 presented above.

Two sets of CCA specimens were prepared from the broken HSLA-100 SE(T) specimens. One set of 15 specimens had W=50mm and one set of 7 specimens had W=120 mm. The specimens were tested and analyzed using the E1221 approach. The CCA specimens were conducted at test temperatures of -160 and -150°C, near the initiation reference temperature for the material. The W=120 mm specimens were also instrumented with strain gage rosettes in a manner similar to the SE(T) specimens. The strain gage data was used to prescribe the crack position and velocity in a dynamic finite element analysis and the results are compared with the results of the SE(T) in Figure 16.

The crack arrest results for the W=50 mm CCA specimens are compared with the crack arrest results from the SE(T) specimens in Figure 15. The crack arrest reference temperature determined from this set of specimens was -120°C, which is 16°C warmer that the -136°C reference temperature measured using the SE(T) specimens with a dynamic analysis. It should be noted that two of the specimens exhibited very low initiation toughness and consequently have very low arrest values. If these two specimens are considered outliers, then the adjusted T_{KIa} for the W=50 mm CCA specimens is -127°C.

The crack arrest toughness for the W=120 mm specimens was determined using the static analysis of E1221 and also from dynamic FEA using the crack velocity information from the strain gages. The average crack velocity in all of these tests was 380 m/s, which is similar to the crack speeds observed in the SE(T) specimens which were tested at higher temperatures. The results are tabulated in Table 5 and show slight differences between the static and dynamic calculations of the crack arrest toughness for individual specimens. The maximum difference observed was 21% for

specimen GQN-TL5C. There is no systematic trend between the static and dynamic toughness calculations. The averages of both the static and dynamic crack arrest toughness are identical. The dynamic results ranged both higher and lower than the static results. It is interesting to note that despite the differences in the specific crack arrest toughness values, both calculation approaches yield equivalent crack arrest reference temperatures of T_{KIa} = -136°C which is the same value obtained from the SE(T) specimens with the thermal gradients. The full set of crack arrest toughness results for the HSLA-100 alloy steel is plotted in Figure 16. The overall trend in toughness as a function of temperature is well represented by the crack arrest master curve and both the SE(T) specimens with a thermal gradient and the CCA specimens lie on the same curve.

Table 5 Comparison of static analysis (E1221) and dynamic analysis results for the HSLA100 CCA specimen tests.

Specimen	Test Temperature (°C)	K_{Ia} E1221 (MPa-$m^{1/2}$)	K_{IA} FEA (MPa-$m^{1/2}$)
GQN-TL4C # 1	-160	65.9	69.1
GQN-TL4C # 2[a]	-160	58.5	64.8
GQN-TLXC	-160	76.4	86.1
GQN-TL7C	-150	73.5	71.8
GQN-TL7AC	-150	65.7	67.7
GQN-TL5C [b]	-150	87.8	69.6
GQN-TLYC	-150	77.1	73.8
GQN-TL4AC # 1 [b]	-150	80.2	75.6
GQN-TL4AC # 2 [a]	-150	79.3	87.4
T_{KIa} (°C)		**-136**	**-136**

[a] short crack jump, specimen tested twice
[b] strain gage data not recorded, velocity assumed

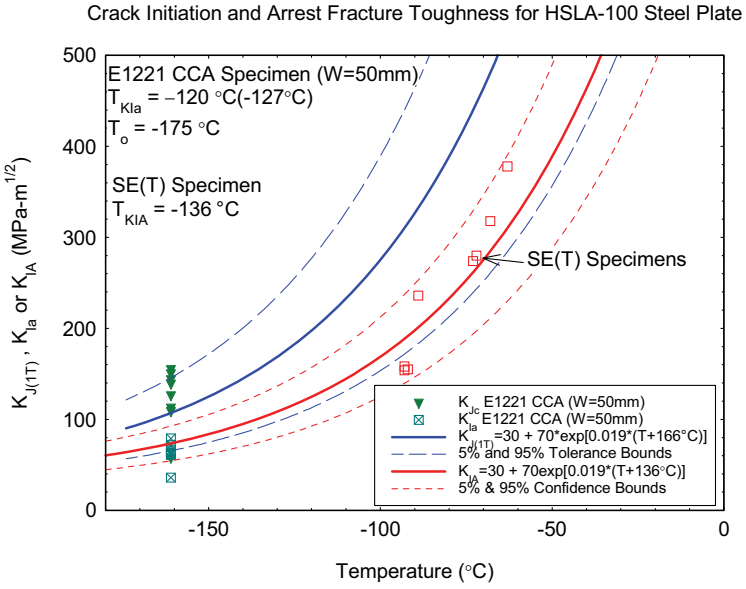

Figure 15 Crack initiation and arrest toughness of HSLA-100 from 1T (W=50 mm) CCA specimens compared with master curves for HSLA-100.

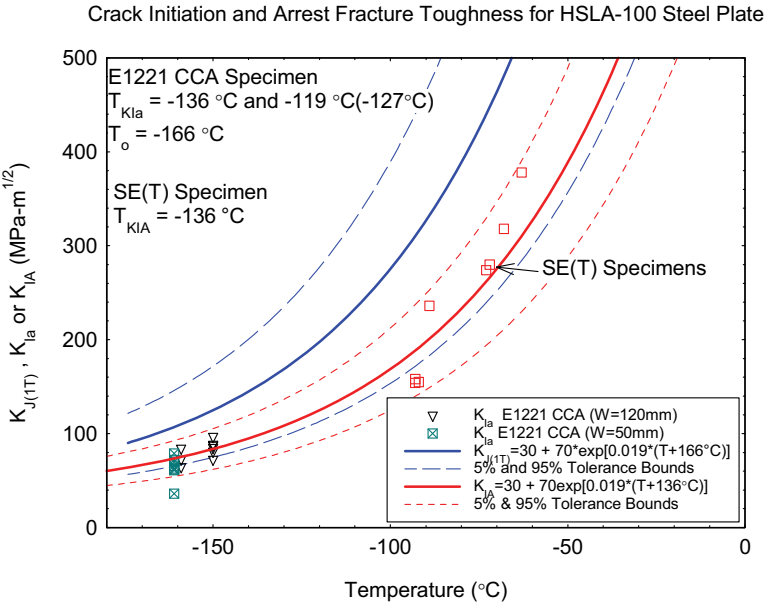

Figure 16 Crack arrest toughness of HSLA-100 determined from CCA specimens compared with master curves.

Euro Forging Steel. Two sets of CCA specimens with W=50 mm and W = 110 mm were prepared from a piece of the Euro forging. Standard crack arrest tests using precracked specimens were conducted in accordance with E1221 at temperatures from -120°C to -80°C, close to the crack initiation reference temperature for this material, T_o = -90°C. The W=110mm specimens were instrumented with strain gages to determine the crack velocity for input into dynamic finite element analyses of these tests. Successful crack arrest was achieved in eleven of the sixteen W=50 mm specimens and in four of the eight W=110 mm specimens. At the lowest temperatures, the cracks either ran too far through the specimen or branched after a few millimeters of brittle crack extension. The results from the E1221 analysis of these tests are plotted in Figure 17. The crack arrest reference temperature, T_{KIa}, was calculated to be -16°C for this material.

Strain gage data was successfully recorded for two of the W=110 mm specimens and dynamic finite element analysis was performed for those tests. In one case, the predicted strains showed fairly good agreement with the measured strain signals as shown in Figure 18 for specimen EUR-4A. However, the dynamic crack arrest toughness was calculated to be 25% lower than that computed using the E1221 procedure, 32 to 43 MPa-$m^{1/2}$ at -95°C. The calculated crack driving force history is plotted in Figure 19. The large difference between the FEA predictions and the static calculations is due in part to the large increase in CMOD measured on the specimen during the run-arrest event. The brittle fracture initiated at a CMOD = 0.48 mm and the CMOD increased an additional 50% after initiation. This large increase in CMOD was not predicted in the finite element analysis, nor was it observed in any of the other tests In fact, the FEA predicted a very sight decrease in CMOD for this test. If the CMOD was assumed to remain constant during the run arrest event, there is much better agreement between the dynamic FEA value of crack arrest toughness and the E1221 value with K_{Ia} = 35.8 MPa-$m^{1/2}$ which is much closer to the value of 32 MPa-$m^{1/2}$ from the finite element analysis.

For the second specimen, there was rather poor agreement between the predicted and measured strains but good agreement between the crack arrest toughness computed using the static approach and the dynamic FEA predictions, 49 (dynamic) and 46.8 MPa-$m^{1/2}$.

Wallin [5] developed an empirical relationship between the crack initiation reference temperature, T_o, and the shift between the crack initiation and crack arrest reference temperatures, T_{KIa} - T_o, by analyzing the results of many crack arrest tests in the literature. For the original model, all steels had a nickel content less than 1.2%. A subsequent model [15]included the effect of additional nickel on the shift. The results presented in this paper are plotted vs. the model and original data used to develop the relationship in Figure 20. The models do a respectable job of predicting the shift in the reference temperature. For the Euro forging material, it is worth noting that there was considerable variability in the T_o values reported for this forging with results ranging from -109°C to -85°C[15].

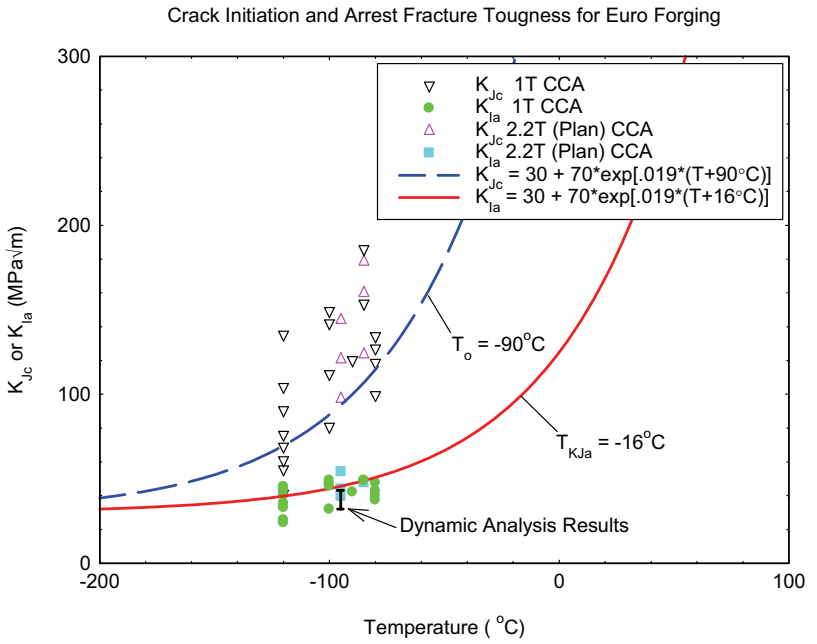

Figure 17 Summary of E1221 static crack arrest results for the Euro forging material**.**

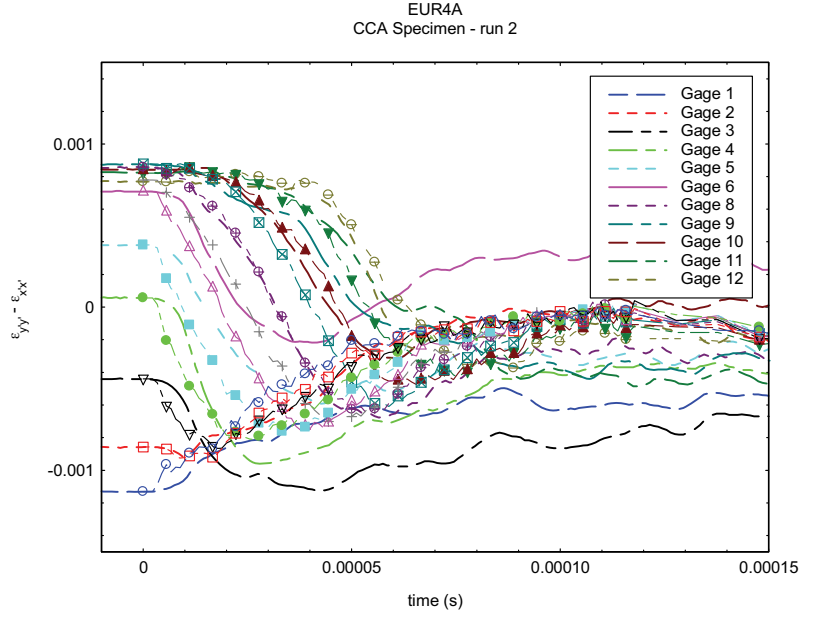

Figure 18 Comparison of the measured and predicted strains for a Euro material CCA specimen. The curves with the symbols are the predicted response.

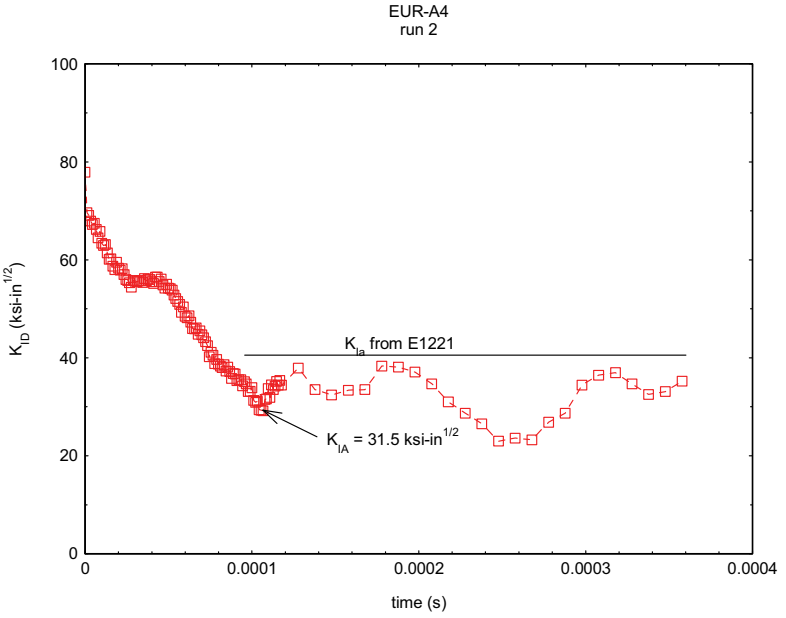

Figure 19 The predicted dynamic crack driving force vs. time for specimen EUR-4A compared with K_{Ia} determined using E1221 approach.

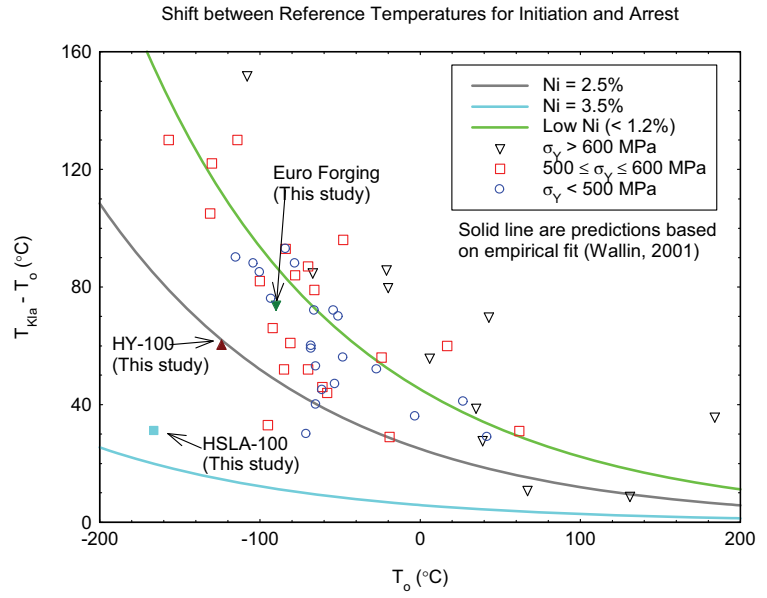

Figure 20 The predicted shift in reference temperature between crack initiation and arrest as a function of the reference temperature along with the results from this study.

Conclusions

SE(T) crack arrest specimens utilizing a thermal gradient to arrest the crack provide a useful alternative for structural steels with high cleavage initiation toughness. While the tests are more involved and expensive to run and analyze, a majority of the tests are successful, demonstrating limited crack tunneling and improved in-plane behavior of cleavage crack in comparison with that of the typical ASTM E1221 compact crack arrest specimen. The dynamic analysis required to obtain viable crack arrest measurements is complex, but within the capabilities of available fracture mechanics analysis packages and can be accomplished on ordinary personal computers.

Application of the dynamic finite element analysis to isothermal ASTM E1221 compact crack arrest specimens was also successful providing a valuable linkage between the dynamic SE(T) test analysis and the standard, static analysis of E1221.

Excellent agreement was found between the results of E1221 style tests which use a static K_{Ia} evaluation technique and the dynamic analysis results used for the SE(T) specimen tests, giving results that agreed within 0 to 9°C.

E1221 style crack arrest tests conducted on the Euro forging material were successful, though as is often the case, many individual tests were invalid because of crack branching, crack tunneling, failure of a crack to initiate, or failure of the crack to arrest.

Dynamic analysis of CCA specimens of the Euro material was less successful due to the large additional crack opening that occurred prior to arrest in one of the specimens. This behavior was not commonly observed in other tests and it was not predicted in the finite element analysis.

References

[1] Naus, D.J., et al., "Crack-Arrest Behavior in SEN Wide Plates of Quenched and Tempered A533 Grade B Steel Tested Under Nonisothermal Conditions," NUREG/CR-4930, U.S. Nuclear Regulatory Commission, Washington, D.C, August 1987.

[2] Naus, D.J., Keeney-Walker, J., Bass, B.R., Bolt, S.E., Fields, R.J., deWitt, R., Low, S.R. III, "High-Temperature Crack-Arrest Behavior in 152-mm-Thick SEN Wide Plates of Quenched and Tempered A533 Grade B Class 1 Steel," NUREG/CR-5330, U.S. Nuclear Regulatory Commission, Washington, D.C., April 1989.

[3] Kalthoff, J.F., Beinert, J., Winkler, S., and Klemm, W., "Experimental Analysis of Dynamic Effects in Different Crack Arrest Test Specimens," Crack Arrest Methodology and Applications, ASTM STP 711, G.T. Hahn and M.F. Kanninen, Eds., American Society for Testing and Materials, 1980, pp. 109-127.

[4] Kobayashi, T. and Dally, J.W., "Dynamic Photoelastic Determination of the a(dot)-K Relation for 4340 Alloy Steel," Crack Arrest Methodology and Applications, ASTM STP 711, G.T. Hahn and M.F. Kanninen, Eds., American Society for Testing and Materials, 1980, pp. 189-210.

[5] Wallin, K. and Rintamaa, R. "Master Curve Based Correlation Between Static Initiation Toughness, K_{Ic} and Crack Arrest Toughness, K_{Ia}," 24th MPA-Seminar, Stuttgart, October 8-9, 1998.

[6] Slater, S., et al., "An energy balance approach to crack arrest," European Commission Report, EUR-20952EN, The European Commission, 2004.

[7] Gudas, J.P., "Micromechanisms of fracture and crack arrest in two high strength steels," PhD Dissertation, The Johns Hopkins University, Baltimore, MD 1985.

[8] Wallin, K., (2004) "Inhomogeneity Check of the "EURO" Fracture Toughness Reference Data Set," *Advance Fracture Mechanics of Life and Safety Assessments - ECF 15*, August 11-13, 2004, Stockholm, Sweden.

[9] Joyce, James A., and X. Gao, "Analysis of Material Inhomogeneity in the European Round Robin Fracture Toughness Data Set," presented at the Seventh International ASTM/ESIS Symposium on Fatigue and Fracture, Tampa, 2007.

[10] Dally, J. W. and Sanford, R. J., "Strain Gage Methods for Measuring the Opening Mode Stress Intensity Factor, K_I," *Experimental Mechanics*, Vol. 27, No. 4, 1987, pp. 381–388.

[11] Gullerud, A.S., Koppenhoefer, K.C., Roy, A. and Dodds, R.H., Jr., "Warp3D: 3−D Dynamic Nonlinear Fracture Analysis of Solids Using Parallel Computers and Workstations," Report No. UILU−ENG−95−2012, University of Illinois, February 2004.

[12] Link, R.E., "Analysis of Dynamic Fracture and Crack Arrest of an HSLA Steel in an SE(T) Specimen," *Journal of ASTM International*, Vol. 3, No. 1, Paper ID JAI13236, January 2006.

[13] Link, R.E. and Roe, C., "Crack Arrest Testing Using Small Wide Plate SE(T) Specimens," *Journal of ASTM International*, Vol. 5, No. 3, 2008, Paper ID JAI101001.

[14] Freund, L.B., Dynamic Fracture Mechanics, Cambridge University Press, 1990.

[15] Wallin, K., "Correlation Between Static Initiation Toughness K_{Jc} and Crack Arrest Toughness K_{Ia}," *Fatigue and Fracture Mechanics: 32nd Volume, ASTM STP 1406*, R.C Chona, Ed., American Society for Testing and Materials, West Conshohocken, PA, 2001, pp. 17-34.